Algal Research 98 (2026) 104894

Contents lists available at ScienceDirect

Algal Research

journal homepage: www.elsevier.com/locate/algal

The transmembrane domain is a primary determinant of the location and substrate specificity in cyanobacterial FtsH heterocomplexes

Lanbo Yi [a,b], Natalia Kulik [c], Shengxi Shao [d], Peter J. Nixon [e], Josef Komenda [c], Vendula Krynická [c,*], Jianfeng Yu [e,*], Bin Liu [f,**]

[a] School of Mechanics and Engineering Science, Peking University, Beijing, 100871, China
[b] Shenzhen Key Laboratory of Food Nutrition and Health, Institute for Innovative Development of Food Industry, College of Chemistry and Environmental Engineering, Shenzhen University, Shenzhen, 518071, China
[c] Centre Algatech, Institute of Microbiology, Czech Academy of Sciences, 37981, Trebon, Czech Republic
[d] Nanchang University–Imperial College London Joint Laboratory on Photosynthesis and Low Carbon Biotechnology, Key Laboratory of Poyang Lake Environment and Resource Utilization Ministry of Education, Nanchang University, Nanchang, 330031, China
[e] Sir Ernst Chain Building-Wolfson Laboratories, Department of Life Sciences, Imperial College London, SW7 2AZ, London, United Kingdom
[f] Yantai Key Laboratory of Characteristic Agricultural Bioresource Conservation & Germplasm Innovative Utilization, School of Life Sciences, Yantai University, Yantai, 264006, China

ARTICLE INFO

Keywords:
FtsH protease
Transmembrane domain
Substrate specificity
Membrane localization
Photosystem II repair
Functional divergence

ABSTRACT

Membrane-embedded FtsH proteases play important and diverse physiological roles in prokaryotes, chloroplasts and mitochondria, but how substrates are distinguished remains unclear. The cyanobacterium *Synechocystis* sp. PCC 6803 contains four FtsH homologs organized into two distinct heterocomplexes and one homocomplex. The two heterocomplexes, derived from a recent gene duplication event, are the essential FtsH1/3 complex found in the cytoplasmic membrane, and the thylakoid-embedded FtsH2/3 complex, with a role in the repair of photodamaged photosystem II. Using a domain swapping approach, we demonstrate here that the transmembrane domains of FtsH1 and FtsH2 are primary determinants of the cellular location and functional differences between the FtsH1/3 and FtsH2/3 complexes, whereas the soluble AAA+ (ATPases associated with diverse cellular activities) and protease domains and the soluble linker were largely interchangeable under the conditions tested. Overall, our findings identify the transmembrane domain as an important determinant of both the location and substrate specificity of FtsH heterocomplexes and support a role for this domain in their functional evolution.

1. Introduction

FtsH proteases are ubiquitous membrane-anchored, ATP-dependent metalloproteases with diverse roles in cellular function. Many FtsH isoforms selectively degrade membrane and soluble proteins and have specialized functions in regulating photosynthesis, respiration and cellular differentiation in mammals and plants [1].

A typical FtsH molecule comprises three domains: an N-terminal transmembrane domain serving as a membrane anchor, followed by an AAA+ (ATPases associated with diverse cellular activities) domain that enables substrate translocation into the complex via ATP hydrolysis, and a C-terminal zinc-binding M41 domain that cleaves substrates into peptides [2,3]. Structural studies show that FtsH subunits assemble into hexameric complexes in the membrane, with each domain flanked by its counterparts from the adjacent protomers [3–5]. In organisms with multiple FtsH homologs, different homologs form distinctive heterocomplexes with specialized functions [6–9].

Although the proteolytic mechanism of FtsH complexes is considered highly conserved, how FtsH homologs distinguish between substrates remains elusive [1]. The conserved Phe-Val-Gly (FVG) motif aligned at the center of the AAA+ ring is the primary contact point to feed substrates into the AAA+ chamber. The unfolded peptide chain then reaches the M41 peptidase site to be cleaved into short peptides [3,4]. The geometry of the opening through which substrates reach the FVG motif has been implicated in substrate access [5,10,11]. This geometry may be influenced by the properties of the membrane and AAA+ domain surfaces [12–15], and linker properties can modulate conformational flexibility and substrate processing [10,11].

* Corresponding authors.
** Correspondence to: B. Liu, School of Life Sciences, Yantai University, No. 1 Siping Road, Huang-Bohai New Area, Yantai, 264006, Shandong Province, China.
E-mail addresses: krynicka@alga.cz (V. Krynická), j.yu@imperial.ac.uk (J. Yu), liubincoe@pku.edu.cn (B. Liu).

https://doi.org/10.1016/j.algal.2026.104894
Received 26 June 2026; Received in revised form 20 July 2026; Accepted 8 August 2026
Available online 10 August 2026

In the model cyanobacterium *Synechocystis* sp. PCC 6803 (hereafter *Syn*6803), the four encoded FtsH homologs form two heterocomplexes (FtsH1/3, FtsH2/3) and one homocomplex (FtsH4) with different substrate specificities [8,16]. Notably, the FtsH1/3 complex located in the cytoplasmic membrane degrades the soluble Ferric Uptake Regulator (Fur), involved in iron stress responses [17,18] and the FtsH2/3 complex, located in the internal thylakoid membrane, degrades damaged D1 protein during photosystem II (PSII) repair and the soluble glucosylglycerol-phosphate synthase (GgpS) involved in osmoprotection [8,19,20]. The FtsH4 homocomplex, also in the thylakoid membrane, degrades high light-inducible proteins (Hlips) and PSI-related proteins [21,22]. Mutational studies have shown that FtsH1 and FtsH3 are essential for cell viability [23] whereas loss of FtsH2 impairs photoautotrophic growth but enhances resistance to osmotic stress [20,24], and FtsH4 disruption increases sensitivity to high-light and low-temperature stresses [16].

Phylogenetic analyses have shown that FtsH1 and FtsH2 arose via gene duplication and are the most recently diverged FtsH homologs [25]. In this study, we used a domain swapping approach to identify the structural features in FtsH1 and FtsH2 that are important for their different substrate specificities and membrane locations. Our data show that the transmembrane domain is a primary determinant of these differences, while swapping the linker, AAA+ and protease domains had little detectable effect on the FtsH2-dependent phenotypes tested here. Overall, our results highlight the importance of the transmembrane domain for the functional divergence of FtsH heterocomplexes in cyanobacteria.

2. Materials and methods

2.1. Strains and growth conditions

The glucose-tolerant GT-P substrain of *Syn*6803 was used as the wild-type (WT) background. All other strains used in this study were derived from this background as described below. Unless otherwise specified, strains were maintained at 30 °C under continuous illumination (20 μE m^{-2} s^{-1}) in BG11 medium supplemented with 5 mM glucose. Liquid medium contained 5 mM TES–KOH (pH 8.2), whereas solid medium contained 10 mM TES–KOH (pH 8.2), 1.5% (*w*/*v*) agar, and 0.3% (w/v) sodium thiosulfate. Liquid cultures were grown in 250 mL or 1 L Erlenmeyer flasks shaken at 220 rpm. When required, BG11 medium was supplemented with the iron chelator deferoxamine (DFB), maltose, or lincomycin at the concentrations specified in the relevant sections.

2.2. Construction of FtsH mutant strains

In *Syn*6803, the four FtsH homologs, FtsH1–FtsH4, correspond to the locus tags *slr1390*, *slr0228*, *slr1604*, and *sll1463*, respectively. Four categories of *Syn*6803 mutant strains targeting *ftsH1* and/or *ftsH2* loci were generated in this study: (i) an *ftsH2* knockout strain (Δ*ftsH2*), (ii) chimeric FtsH strains, (iii) GFP-labeled strains for membrane localization studies, and (iv) *ftsH1* knockout strains (Δ*ftsH1*) in selected complemented backgrounds. Our method parallels established plasmid-based genome-editing approaches in *Syn*6803 [26], with modifications that enabled domain-swapped constructs following deletion of *ftsH2*, thereby generating markerless mutants expressing chimeric FtsH proteins.

All plasmid constructs were generated using the pVB backbone (2531 bp), derived from pRSET-A. Flanking regions (~445 bp upstream and ~ 555 bp downstream) of each target locus, as well as FtsH domain fragments described below, were PCR-amplified from WT genomic DNA using primers incorporating *Bsm*BI, *Bsa*I, or *Bsp*MI restriction sites. A complete primer list is provided in Table S3. Genomic DNA was extracted using a bacterial/fungal DNA extraction kit (Zymo Research, USA). PCR amplifications were performed with Q5 High-Fidelity DNA Polymerase (New England Biolabs, USA; hereafter NEB). PCR products and assembled plasmids were purified using commercial kits (Promega, USA; Omega Bio-Tek, USA) and verified by Sanger sequencing.

To generate the Δ*ftsH2* mutant, the upstream and downstream flanking regions of the *ftsH2* locus were cloned into the pVB vector using *Bsp*MI restriction sites. An *Eco*RV site introduced between the two flanking regions enabled insertion of a kanamycin–sacB cassette, allowing antibiotic selection followed by sucrose-based counterselection (Fig. S8).

To investigate domain interchangeability, a series of chimeric FtsH strains was constructed in the Δ*ftsH2* background (Fig. S8). FtsH domain fragments were amplified using primers incorporating *Bsm*BI restriction sites. A codon-optimized 3 × FLAG tag was generated by annealing complementary oligonucleotides. The amplified fragments and 3 × FLAG tag were then assembled into various domain-swapped combinations in the pVB backbone carrying the *ftsH2* flanking regions, using a single-step, multi-fragment Golden Gate assembly protocol (NEB).

Chimeric strain names were assigned according to domain origin. The leading numeral 2 indicates an FtsH2-derived construct expressed from the *ftsH2* locus, whereas T, L, A, and P denote the transmembrane, linker, AAA+, and protease domains, respectively. The number following each domain letter indicates the FtsH homolog from which that domain was derived; for example, strain 2A1 contains the AAA+ ATPase domain of FtsH1 in place of the corresponding domain of FtsH2. Detailed strain nomenclature and genotypes are provided in Table S1.

For localization analyses, the 3 × FLAG tag was replaced with a flexible glycine-serine linker (GGGGS) fused to superfolder GFP. These constructs carried either full-length FtsH–GFP fusions or domain-swapped FtsH–GFP variants. This strategy was conceptually similar to previously described FtsH–GFP fusions [27], with additional domain swaps to test effects on subcellular localization.

Because deletion of native *ftsH1* is not possible in WT cells [23], Δ*ftsH1* strains were generated only in backgrounds expressing chimeric or alternative FtsH proteins from the *ftsH2* locus. To generate Δ*ftsH1* strains, homologous regions upstream (~445 bp) and downstream (~555 bp) of *ftsH1* were amplified with *Bsa*I sites. These fragments, flanking a chloramphenicol–sacB cassette, were assembled into the pVB vector to produce the Δ*ftsH1* plasmid.

All constructs were introduced by natural transformation. Δ*ftsH2* and Δ*ftsH1* strains were selected on kanamycin (50 μg·mL^{-1}) or chloramphenicol (30 μg·mL^{-1}), respectively. Markerless 3 × FLAG- or GFP-tagged strains were recovered by 5% (*w*/*v*) sucrose counterselection. For Δ*ftsH1* strains, successful knockout was further confirmed by PCR after prolonged (>4 months) growth without selective pressure, and the absence of the FtsH1 protein was validated by immunoblotting.

2.3. Cell absorption spectra and chlorophyll quantification

Whole-cell absorption spectra were recorded at room temperature with a UV-3000 spectrophotometer (Shimadzu, Japan). For chlorophyll measurements, pigments were extracted from pelleted cells with absolute methanol, and chlorophyll concentrations were determined as described previously [28].

2.4. Preparation of crude membranes

Harvested cells were flash-frozen in liquid nitrogen and stored at −80 °C. Cell pellets were washed and resuspended in ice-cold KPN buffer containing 40 mM potassium phosphate (pH 8.0), 100 mM NaCl, 1.4 mM β-mercaptoethanol, and EDTA-free Enhanced Protease Inhibitor Cocktail (Proteintech, USA). Cells were disrupted for 10 min using a bead mill (TissueLyser II, QIAGEN, Germany) by mixing equal volumes of cell suspension and beads composed of a 1:1 (*v*/*v*) mixture of 0.1-mm glass beads (Sigma-Aldrich, USA) and 0.1-mm zirconium oxide beads (Servicebio, China). Crude membranes were isolated by centrifugation at 21,000 ×*g* for 30 min at 4 °C and resuspended in fresh KPN buffer containing protease inhibitors. The chlorophyll concentration of the

resuspended membranes was measured spectrophotometrically, and samples were adjusted to 1 μg chlorophyll μL^{-1} and stored at −80 °C until use.

2.5. Isolation of FLAG-tagged FtsH proteins

FLAG-tagged FtsH chimeric proteins were isolated from 100 μL crude membrane fractions (1 μg chlorophyll μL^{-1}) prepared as described above. Membrane fractions were solubilized with 1% (*w/v*) n-dodecyl β-D-maltoside (DDM) for 30 min at 4 °C and clarified by centrifugation at 21,000 ×*g* for 30 min. The clarified supernatant was incubated with anti-FLAG M2 Magnetic Beads (Merck, USA) for 3 h at 4 °C. Beads were then washed four times with 500 μL of Tris-buffered saline (TBS) containing 0.03% (*w/v*) DDM. FLAG-tagged proteins were eluted three times, each for 30 min at 4 °C, with 200 μL TBS containing 150 μg mL^{-1} 3 × FLAG peptide (Beyotime Biotechnology, China) and 0.03% (w/v) DDM. Combined eluates were concentrated to approximately 50 μL using a 100 kDa MWCO ultrafiltration device (Millipore, USA), yielding samples corresponding to crude membranes containing 2 μg chlorophyll μL^{-1}. Sample amounts are expressed as chlorophyll equivalents based on initial membrane fractions to facilitate direct comparisons.

For Δ*ftsH1* samples, flow-through fractions from bead incubations were also collected and concentrated to approximately 50 μL using 30 kDa MWCO ultrafiltration devices (Millipore, USA), yielding samples corresponding to crude membranes containing 2 μg chlorophyll μL^{-1}. Samples were stored at −80 °C until analysis.

2.6. Protein electrophoresis and immunoblotting

FtsH chimeric proteins purified as described above were separated by SDS-PAGE using 10% resolving gels containing 6 M urea at 120 V for 2.5 h. Purified samples were loaded onto gels at amounts equivalent to 5 μg chlorophyll from the original crude membranes per lane, except for the 2 T1 strain, for which twice this amount was loaded due to lower detection efficiency. Prior to loading, samples were incubated for 1 h at room temperature in loading buffer containing 62.5 mM Tris-HCl (pH 6.8), 10% (*v/v*) glycerol, 2% (*w/v*) SDS, 0.5% (w/v) bromophenol blue, and 5% (v/v) β-mercaptoethanol. Duplicate gels were either silver-stained or transferred onto PVDF membranes at a constant current of 400 mA for 90 min for immunoblotting. Transfer was performed using carbonate-based transfer buffer containing 3 mM Na_2CO_3, 10 mM $NaHCO_3$, and 20% (v/v) ethanol.

Membranes were blocked with 5% (w/v) nonfat milk in TBS containing 0.1% Tween-20 (TBST) for 1 h at room temperature and incubated with the appropriate primary antibodies for 1 h at room temperature. After washing with TBST, proteins were detected using a Luminol enhancer kit (Thermo Fisher Scientific, USA), and images were captured with a ChemiDoc XRS+ imaging system (Bio-Rad Laboratories, USA).

Additional immunoblots assessing in vivo degradation or accumulation of D1, Fur, and IsiA in response to expression of FtsH chimeric proteins were performed as described previously [18].

Crude membrane samples, flow-through fractions, and FLAG-purified eluates from control and Δ*ftsH1* strains were also immunoblotted with anti-FtsH1 antibody to confirm the knockout of native FtsH1.

For two-dimensional (2D) gel analyses, samples were normalized based on equal cell numbers. Crude membranes were then isolated as described above and first separated by clear native (CN)-PAGE using 4–14% gradient gels according to the published protocol [29]. Following CN-PAGE, individual protein complexes were resolved by incubating gel strips from the first dimension in denaturing solution containing 2% (*w/v*) SDS and 1% (w/v) dithiothreitol at room temperature for 30 min. Proteins were then separated in the second dimension by SDS-PAGE on 12–20% linear gradient gels containing 7 M urea. Gels were stained with SYPRO Orange (Sigma-Aldrich, USA) or transferred onto PVDF membranes for immunoblot analyses. After transferring proteins from the second-dimension gels and incubating membranes with antibodies, chemiluminescent signals were detected using Immobilon Crescendo substrate (Millipore, USA) and imaged by an LAS-4000 camera (Fujifilm).

Primary antibodies used in this study recognized D1 [30], IsiA and Fur [18], FtsH1, FtsH3, FtsH4 and all FtsH isoforms [27], FtsH2, and FLAG tag (Thermo Fisher Scientific, USA). The custom anti-FtsH2 antibody was commercially generated by Proteintech (Wuhan Sanying Biotechnology, China) using a synthetic peptide antigen (Cys-DAQVRQLAEQGHQMARK, residues 564–580 of *Syn*6803 FtsH2) and affinity-purified from rabbit antisera.

2.7. Spot growth assays under different light intensities or non-salt osmotic stress

Cells grown to logarithmic phase were harvested and adjusted to an OD750 of 1.0. Serial dilutions (0.1, 0.01, and 0.001) were prepared, and aliquots (6 μL) of each dilution were spotted onto BG11 plates with or without 5 mM glucose. Plates were incubated at 30 °C under four distinct light intensities: low (5–10 μE m^{-2} s^{-1}), medium (30–40 μE m^{-2} s^{-1}), medium-high (70–90 μE m^{-2} s^{-1}), and high (110–130 μE m^{-2} s^{-1}). Colony growth was photographed once clear phenotypic differences between strains became apparent. Typical incubation periods for plates without glucose were approximately 15 days under low light, 6 days under medium and medium-high light, and 4 days under high light conditions. For plates containing glucose, incubation times were shorter: approximately 6 days under low light, and 4 days under medium, medium-high, and high light conditions.

For non-salt osmotic stress assays, cells were prepared and serially diluted as described above. Aliquots (6 μL) of each dilution were spotted onto BG11 plates containing 5 mM glucose with or without 300 mM maltose. Plates were incubated at 30 °C under continuous illumination of 20 μE m^{-2} s^{-1}. Colony growth and tolerance to maltose-induced osmotic stress were documented photographically once clear differences in growth phenotypes were observed (typically after 4–6 days).

2.8. Structural modeling and molecular dynamics simulations

Structural models of FtsH1/3 and FtsH2/3 complexes were initially generated using AlphaFold 3 with ATP and Zn^{2+} included [31]. The transmembrane domain of FtsH1 was modeled based on homology to FtsH3 using MODELLER [32], and domain arrangements were inspected and adjusted using YASARA [33]. The position of each complex within the membrane was determined using the OPM 2.0 server [34]. Membrane embedding and preparation of simulation systems for molecular dynamics (MD) were performed using CHARMM-GUI [35–37]. Subsequent MD simulations and structural analyses were conducted with GROMACS 2021.4 [38,39].

The tilt angle of the FtsH AAA+ ring relative to the membrane plane was quantified by measuring the angle between two reference planes defined by the Cα atoms of residue G12 (membrane plane) and residue L370 (AAA+ ring) of the FtsH3 subunits. Additionally, the gap distance between the substrate-binding site (FVG motif, represented by the Cα atom of residue F234) and the membrane boundary on the substrate-facing side (defined by the Cα atoms of residue S134 in each of the three FtsH3 subunits) was calculated for both FtsH1/3 and FtsH2/3 complexes. Data presented represent averages calculated over the stable simulation interval from 300 to 1000 ns.

2.9. Sequence alignment and linker analysis

Pairwise sequence alignments of *Syn*6803 FtsH2 with FtsH1, FtsH3, and FtsH4 were conducted using the EMBOSS Needle tool (EMBL-EBI). Amino acid differences in the FtsH2 AAA+ ATPase domain (residues 160–415), categorized as either semi-conservative substitutions or non-

conserved residues considered potentially functionally relevant, were mapped onto the predicted structure of the FtsH2/3 complex using PyMOL software.

A previously established dataset comprising 412 cyanobacterial FtsH sequences was used for broader comparative analyses [25]. Isoform-specific alignments were generated separately for each group of FtsH sequences (FtsH1: 99 sequences; FtsH2: 99 sequences; FtsH3: 102 sequences; FtsH4: 112 sequences) using Jalview 2.11.4.1 with MAFFT. Linker regions in the aligned sequences were identified based on conserved motifs, using the corresponding linker sequences from *Syn*6803 as references. These regions typically began with Arg and terminated with a conserved three-residue Ser-[Lys/Arg]-Ala motif. Linker length distributions were calculated, and conservation and consensus annotations were automatically generated using Jalview. A few exceptionally long linker sequences within the FtsH4 alignment were manually trimmed by removing extra residues that interfered with accurate alignment, ensuring consistency across all four FtsH isoforms.

Residue conservation of FtsH1 and FtsH2 was evaluated using the *ConSurf* server (https://consurf.tau.ac.il/). Analyses were carried out individually for the FtsH1 (99 sequences) and FtsH2 (99 sequences) alignments, as well as for a combined dataset (FtsH1 + FtsH2; 198 sequences). Previously generated structural models of FtsH1/3 and FtsH2/3 hexameric complexes (see above) were uploaded in PDB format, with either the FtsH1 or FtsH2 chain specified as the reference structure. Precomputed multiple sequence alignments (MSAs), generated using Jalview 2.11.4.1 with MAFFT as described above, were provided to ConSurf for each analysis. Conservation scores obtained from ConSurf were mapped onto the corresponding protein complex structures for visualization and interpretation.

2.10. Assessment of PSII repair efficiency

Cultures were treated with the protein synthesis inhibitor lincomycin (100 μg mL^{-1}) and subsequently exposed to photoinhibitory illumination (500 μE m^{-2} s^{-1}) for up to 3 h to induce photodamage. Membrane complexes were isolated immediately before and 3 h after lincomycin addition and analyzed by clear native (CN)-PAGE. Photosystem integrity was then assessed by imaging chlorophyll fluorescence. In parallel, membrane samples collected at 0, 30, 60, and 120 min after lincomycin addition were analyzed by SDS-PAGE and immunoblotting to assess oxidative damage to the D1 protein.

2.11. Confocal microscopy

Confocal imaging was performed on a Nikon A1 HD25 confocal microscope using a CFI Plan Apo λ 100×/1.45 oil DIC N2 objective lens. GFP fluorescence (500–550 nm) and chlorophyll autofluorescence (663–738 nm) were excited simultaneously at 488 nm, provided exclusively by an argon laser, and detected separately as 12-bit images with a resolution of 1024 × 1024 pixels.

3. Results

3.1. The AAA+ domain is functionally interchangeable between FtsH homologs

Previous studies have suggested that the AAA+ domain may be involved in substrate recognition [5,11,15]. Although the AAA+ domain contains multiple conserved regions [2,3], sequence alignments revealed characteristic amino-acid variations unique to each *Syn*6803 FtsH homolog. Structural mapping of these variations indicated that most substitutions cluster on the surface (Fig. S1) and so could impact the surface properties, potentially serving as a mechanism to modulate substrate preference.

To test their functional significance, we constructed a series of mutants in *Syn*6803 in which the AAA+ domain of FtsH2 was replaced by that of FtsH1, FtsH3, or FtsH4 (Fig. 1A and Table S1). All chimeric proteins were fused at the C-terminus to a 3 × FLAG tag and expressed from the native *ftsH2* locus after transforming an *ftsH2* deletion strain. Each chimeric protein was purified via C-terminal FLAG-tag affinity purification (Fig. 1B). Immunoblot analyses revealed that all the chimeras co-purified with FtsH3, but not with FtsH1 or FtsH4, indicating the formation of FtsH2/3-like complexes. In the 2A4 mutant, the FtsH3 signal in the purified fraction appeared noticeably weaker than in the WT-3 × FLAG control (Fig. 1B). This may indicate instability of the complex during purification or less efficient assembly of the complex. Nevertheless, FtsH3 was still detected in the purified fraction, indicating that replacement of the FtsH2 AAA+ domain with that of FtsH4 did not prevent the formation of an FtsH2/3-like variant complex.

The FtsH2/3 complex mediates the degradation of damaged D1 during PSII repair and is important for autotrophic growth and tolerance to high irradiance. To assess the ability of the chimeric mutants to maintain photosynthetic performance, cultures were spotted onto BG11 plates and grown either autotrophically or mixotrophically in the presence of added glucose under medium to high light intensities (Fig. 1C and Fig. S2A). Mutants with substituted AAA+ domains showed growth patterns indistinguishable from wild type (WT), whereas Δ*ftsH2*, lacking functional FtsH2, failed to grow. This demonstrates that AAA+ domains from FtsH1, FtsH3, and FtsH4 can effectively substitute for FtsH2 in supporting WT-like growth across different light intensities, consistent with maintained FtsH2-dependent PSII repair.

We then examined whether swapping the AAA+ domain affected the role of FtsH2 in the response to non-salt osmotic stress. *Syn*6803 primarily responds to salt-based osmotic stress by accumulating glucosylglycerol via upregulation of GgpS [20]. However, under maltose-induced, non-salt osmotic stress, wild-type cells fail to accumulate sufficient glucosylglycerol and cannot survive [20]. Conversely, inactivation of FtsH2 leads to elevated GgpS levels and enhanced basal glucosylglycerol accumulation, conferring maltose tolerance [20]. In our spot assay with 300 mM maltose (Fig. 1D), *ΔftsH2* colonies showed robust growth, whereas WT colonies did not. All chimeric mutants expressing swapped AAA+ domains displayed WT-like sensitivity to maltose stress, consistent with preservation of the physiological role of FtsH2 in GgpS regulation.

Together, these results show that the AAA+ domains of FtsH1, FtsH3, and FtsH4 can functionally substitute for that of FtsH2 with respect to the FtsH2 functions tested.

3.2. The linker regions of FtsH1 and FtsH2 are not major determinants of substrate specificity

The AAA+ module and transmembrane domain are separated by a linker sequence. Multiple studies have suggested that tilting of the AAA+ domain relative to the membrane plane can alter the gap available for substrate access to the central pore [5,10,11]. As cyanobacterial FtsH1 and FtsH2 are the most recently diverged homologs, we examined whether differences in their linker regions might contribute to their functional divergence. In the case of *Syn*6803, the linker sequence spans 18 amino-acid residues (aa) in FtsH1 and 21 aa in FtsH2 (Fig. 2A). A notable difference in this region between FtsH1 and FtsH2 is the absence of a conserved Gly-Gly-Pro (GGP) motif in FtsH1, which is present in all FtsH2 orthologs (Fig. S3). In a recent study of *Pseudomonas* FtsH, linker substitutions and a membrane-proximal Gly-Gly-Gly (GGG) insertion enhanced the processing of selected model substrates [10]. We therefore hypothesized that the GGP motif in FtsH2 might contribute to its function.

Molecular dynamics (MD) simulations were used to compare the predicted tilt angle and the gap between the proteolytic complex and the membrane in the native FtsH1/3 and FtsH2/3 complexes. The FtsH1/3 complex was constrained to a narrower average tilt angle of ~5°, whereas the FtsH2/3 complex appeared more flexible, showing an average predicted tilt of ~26° (Fig. 2B).

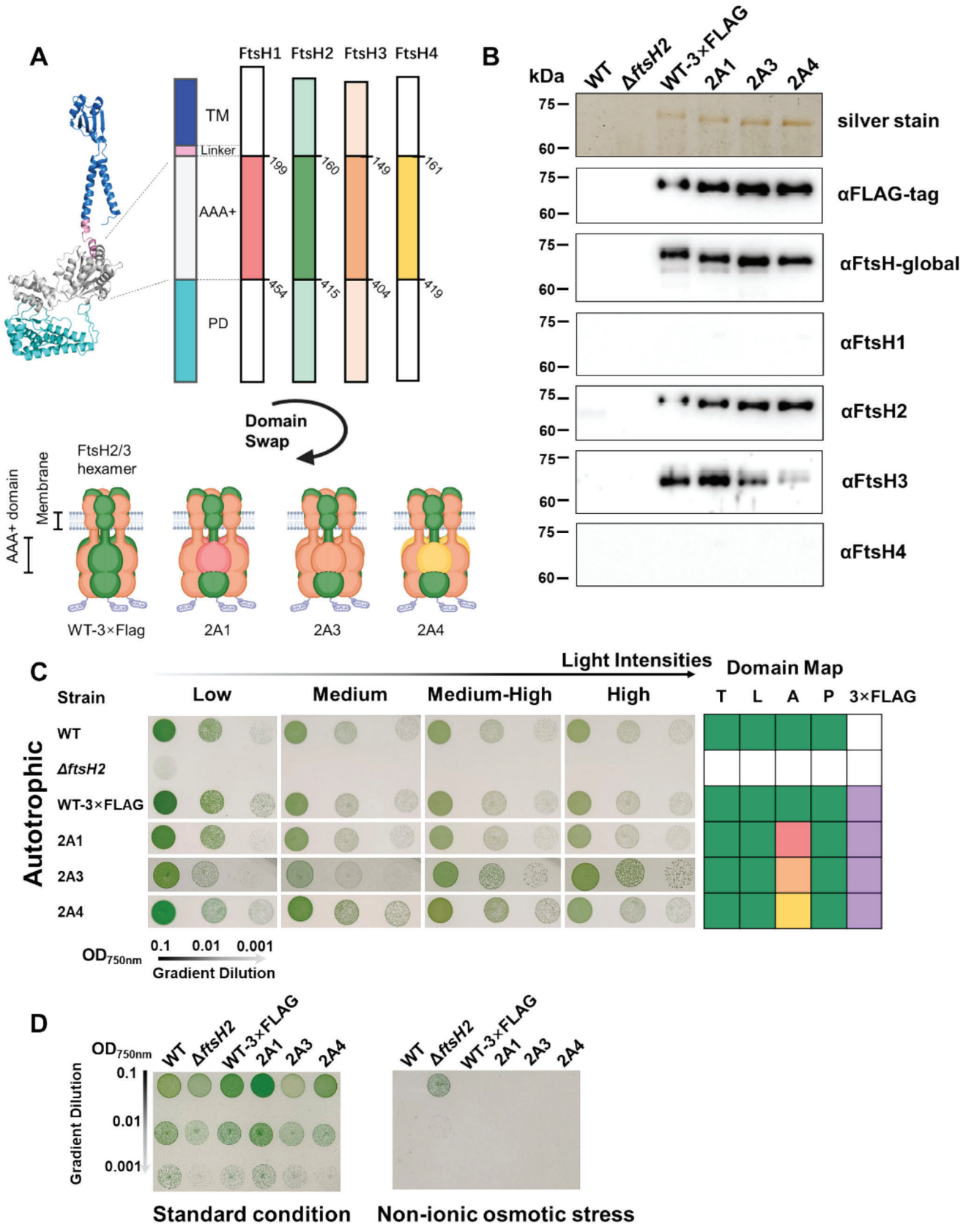

(caption on next page)

Fig. 1. The AAA+ domains of FtsH1, FtsH3, and FtsH4 can substitute for the FtsH2 AAA+ domain.
(A) Strategy for AAA+ domain swapping in *Syn*6803 and predicted architectures of the resulting heterohexamers. The schematic illustrates the modular organization of an FtsH protomer. A linear domain map delineates the transmembrane domain (TM, navy), linker (pink), AAA+ domain (gray), and protease domain (PD, cyan), together with colour-coded AAA+ segments of the four paralogs: FtsH1 (magenta), FtsH2 (green), FtsH3 (orange), and FtsH4 (yellow). Residue boundaries of each donor domain are indicated at right. The AAA+ segment of FtsH2 was replaced by the cognate region of FtsH1, FtsH3, or FtsH4 to generate three chimeric mutants, 2A1, 2A3, and 2A4, each expressing a chimeric FtsH carrying a C-terminal 3 × FLAG tag identical to wild-type (WT-3 × FLAG). The lower panel depicts the predicted in vivo complexes: the native FtsH2/3 heterohexamer and the three chimeric FtsH2/3 assemblies. The substituted AAA+ disk adopts donor coloring; shared TM, linker and PD regions remain those of FtsH2. (B) Silver staining and immunoblot analysis of purified chimeric FtsH complexes using antibodies specific for the FLAG-tag (αFLAG-tag), all FtsH isoforms (αFtsH-global) and each of the isoforms (αFtsH1–4). (C) Spot growth assay under autotrophic conditions across four light intensities (low, 5–10 μE m^{-2} s^{-1}; medium, 30–40 μE m^{-2} s^{-1}; medium-high, 70–90 μE m^{-2} s^{-1}; high, 110–130 μE m^{-2} s^{-1}). The gradient bar below represents OD750 dilutions (0.1, 0.01, 0.001). A chimeric FtsH domain map compares domain configurations across strains. (D) Spot growth assay with or without maltose-induced osmotic stress. Dilution gradients are identical to those in (C). (For interpretation of the references to colour in this figure legend, the reader is referred to the web version of this article.)

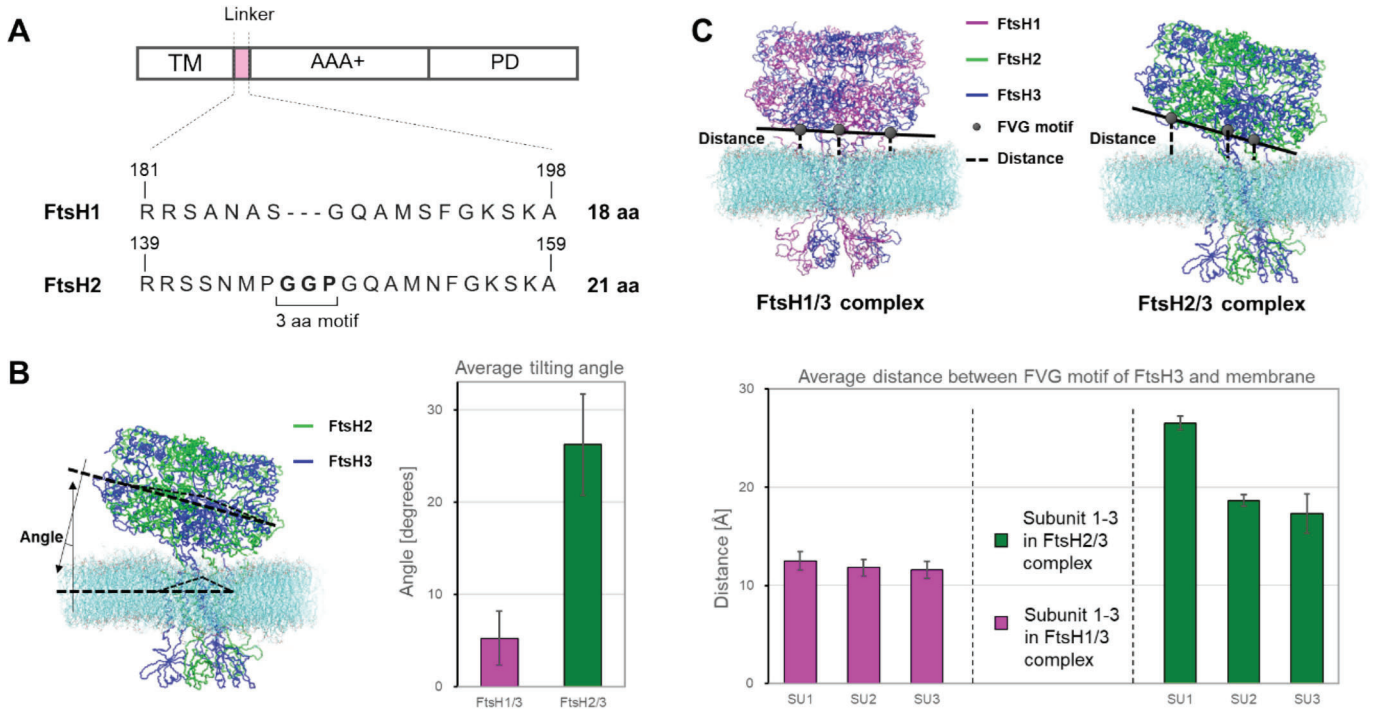

Fig. 2. Differences in sequence and geometry between the FtsH1 and FtsH2 linker regions.
(A) Linear schematic of a model FtsH of *Syn*6803, highlighting flexible linker sequences from FtsH1 (18 aa) and FtsH2 (21 aa). Residues in bold indicate the conserved Gly-Gly-Pro (GGP) motif unique to FtsH2. (B) Illustration of how tilt angles between the AAA+ domain and membrane plane were calculated using the normal vectors defining dihedral planes, exemplified by a snapshot of the FtsH2/3 complex after 1000 ns. Bar plots on the right summarize average tilt angles (± SD) for both FtsH1/3 and FtsH2/3 complexes obtained from molecular dynamics simulations. (C) Gap distances from the substrate-binding Phe-Val-Gly (FVG) to the membrane plane, measured in PyMOL based on conformational changes observed during molecular dynamics simulations, are shown for both FtsH1/3 and FtsH2/3 complexes. Colors indicate FtsH1 (magenta), FtsH2 (green), FtsH3 (blue), and the FVG motif (black spheres). Bar plots at the bottom compare distances from the FVG motifs of the three FtsH3 subunits to the membrane plane in each complex. (For interpretation of the references to colour in this figure legend, the reader is referred to the web version of this article.)

We also measured the vertical distance from the FVG motif at the entrance of the complex to the membrane surface, using the three FtsH3 subunits as internal references (Fig. 2C). In the FtsH1/3 complex, the FVG motifs of the three FtsH3 subunits maintained uniformly short distances (~12 Å) to the membrane. By contrast, the corresponding distances in the FtsH2/3 complex were notably longer and more variable (~17–27 Å). These simulation data suggested that the predicted spatial geometries of the substrate entrances differed markedly between the heterocomplexes. Compared with FtsH1/3, the substrate entrance of the FtsH2/3 complex was predicted to adopt a more wedge-shaped configuration relative to the membrane plane, which may influence substrate access to the central pore.

These predicted differences in tilt angle and gap distance, together with the distinct linker sequences of FtsH1 and FtsH2, prompted us to test whether linker variation might contribute to substrate specificity in vivo. Two *Syn*6803 mutants were constructed in which the FtsH2 linker was modified: mutant 2LΔ has the conserved GGP sequence deleted, resulting in a truncated linker of equal length to that of FtsH1; and mutant 2 L1 has the native 21-aa FtsH2 linker sequence replaced by the 18-aa linker sequence of FtsH1 (Fig. 3A). Both variants copurified with FtsH3 (Fig. 3B), indicating stable heterocomplex formation.

The growth performance of both linker mutants was similar to WT when exposed to medium to high light intensities (Fig. 3C and Fig. S2B) and to maltose stress (Fig. 3D). Consequently, differences in linker length and sequence are not sufficient to explain the functional differences examined between FtsH1 and FtsH2.

3.3. Systematic construction of FtsH mutants with swapped domains

Comparison of primary structures revealed that the transmembrane domain of cyanobacterial FtsH2 paralogs is more conserved than that of FtsH1 paralogs (Fig. S4). To investigate the contribution of the

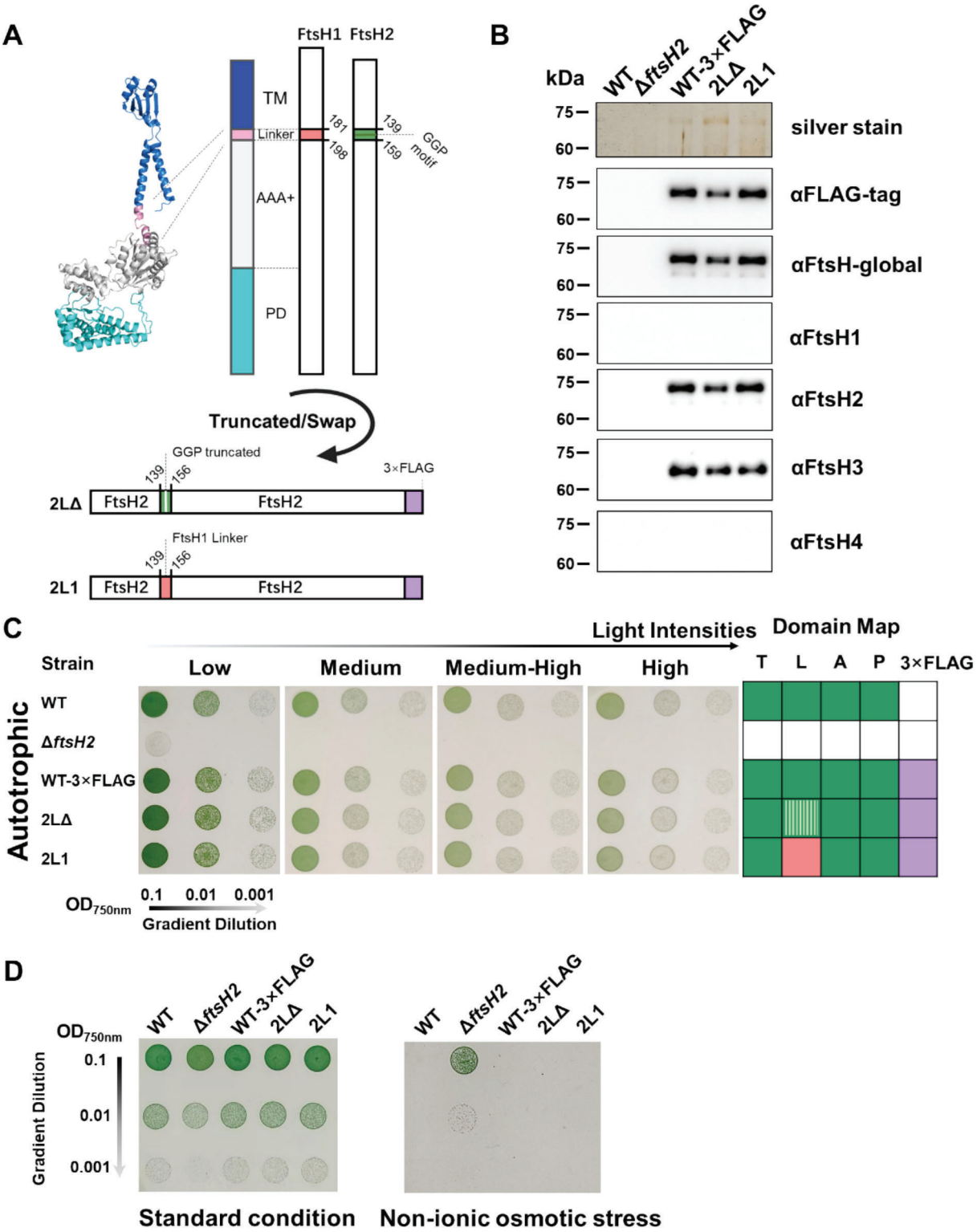

Fig. 3. Mutational analyses confirm that the FtsH1 linker can functionally substitute for the FtsH2 linker in vivo.
(A) The composite schematic (top) depicts a single FtsH protomer (cartoon, left) and, in the center, a linear domain map that defines the transmembrane domain (TM, navy), linker (pink), AAA+ domain (gray), and protease domain (PD, cyan). To the right, the linkers of FtsH1 (magenta) and FtsH2 (green) are aligned, highlighting the GGP motif in FtsH2. Two mutants were constructed: 2LΔ, in which the FtsH2 linker was truncated to match the length of FtsH1 (removing the GGP motif); and 2 L1, in which the entire FtsH2 linker was replaced by that of FtsH1. The lower panel shows the resulting chimeric proteins, each retaining the native FtsH2 backbone and bearing a C-terminal 3 × FLAG tag for subsequent purification. (B) Silver staining and immunoblot analysis of purified chimeric FtsH complexes using antibodies against the FLAG tag, all FtsH isoforms (αFtsH-global), and FtsH1–4. (C) Spot growth assay under autotrophic conditions with the same four light intensities described in Fig. 1C. (D) Spot growth assay under maltose-induced osmotic stress. (For interpretation of the references to colour in this figure legend, the reader is referred to the web version of this article.)

transmembrane domain to the functional differences between *Syn*6803 FtsH1 and FtsH2, we generated a series of mutants in which the transmembrane and the other domains of FtsH2 were replaced by those from FtsH1 (Table S1 and Fig. 4A). Mutants were named according to the domains of FtsH2 replaced in each chimera: T (transmembrane domain), L (linker), A (AAA+ module), and P (protease domain), followed by a number indicating the source domain (1 = FtsH1). Detailed strain nomenclature and genotypes are provided in Section 2.2 and Table S1. All chimeric proteins were isolated via C-terminal FLAG-tag affinity purification and shown to co-purify with FtsH3, confirming their assembly into heterocomplexes (Fig. 4B).

To assess the impact of swapping transmembrane domains on the formation of FtsH complexes, we analyzed the migration patterns of chimeric and native FtsH complexes by two-dimensional electrophoresis (CN-PAGE followed by SDS-PAGE) (Fig. 4C). In the WT samples, FtsH1/3 and FtsH2/3 complexes exhibited clear differences in migration, compared with those observed in Δ*ftsH2* lacking the FtsH2/3 complex and the FtsH1down strain constructed by Krynicka et al. with reduced levels of the FtsH1/3 complex [17]. Migration of the 2L1A1P1 chimera, though slightly shifted, closely resembled that of native FtsH2/3 complexes. In contrast, complexes containing chimera 2 T1 co-migrated with the native FtsH1/3 complex. Overall, these data support the formation of heterohexameric chimeric complexes.

3.4. The transmembrane domain of FtsH2 is a primary determinant of substrate specificity

First, we tested whether domain-swapping affected the photosynthetic capacity of the mutants under a range of autotrophic and mixotrophic conditions at varying light intensities (Fig. 5A and Fig. S2C). All mutants containing the transmembrane domain from FtsH2 retained WT-like growth patterns; however, strains containing the transmembrane domain from FtsH1, such as the control strain 2T1L1A1P1 (FLAG-tagged FtsH1 expressed in the *ftsH2* locus, Fig. 4A) and 2 T1, in which the transmembrane domain of FtsH2 was replaced by that of FtsH1, displayed a similar phenotype to the Δ*ftsH2* mutant, showing impaired autotrophic growth and marked sensitivity to high-light stress.

To confirm effects on the degradation of D1, strains were exposed to excessive light in the presence of lincomycin, a protein synthesis inhibitor, and D1 levels were monitored (Fig. 5B). The Δ*ftsH2* mutant lacked FtsH2 and showed reduced levels of FtsH3, reflecting the absence of the FtsH2/3 complex [8]. By contrast, mutants 2 T1 and 2L1A1P1 expressing chimeric FtsH proteins maintained FtsH3 levels similar to WT during the treatment. In WT cells, the level of D1 protein decreased during this treatment, consistent with FtsH2/3-mediated D1 degradation. Mutant 2L1A1P1 exhibited a similar degradation rate, indicating that the soluble regions of FtsH1 were able to replace the corresponding regions of FtsH2 (Fig. 5B). By contrast, degradation of the D1 protein was retarded in the Δ*ftsH2* and 2 T1 mutants and gave rise to smeared D1 bands on immunoblots consistent with protein oxidation [40].

CN-PAGE of the same lincomycin-treated, excessive light exposed samples showed that the pattern of PSII complexes in mutant 2L1A1P1 closely resembled WT, whereas the 2 T1 mutant and Δ*ftsH2* mutant accumulated the RC47 complex (Fig. 5C), a characteristic intermediate observed when PSII repair is impaired [41]. Together, these results demonstrate that replacement of the FtsH2 transmembrane domain by that of FtsH1 impairs FtsH2-dependent D1 degradation during PSII repair, resulting in pronounced photosensitivity.

Next, we evaluated whether replacing the transmembrane domain affects FtsH2-mediated osmotic regulation. Maltose-stress assays showed that mutants 2 T1 and 2T1L1A1P1 exhibited enhanced tolerance to 300 mM maltose (Fig. 5D), a phenotype previously associated with FtsH2 inactivation and altered GgpS regulation [20]. Replacement of other domains had no detectable effect on this phenotype, supporting their functional interchangeability.

3.5. Role of the transmembrane domain of FtsH1 in function

We then investigated whether the chimeric 2 T1/FtsH3 complex could substitute for the essential function of FtsH1/3. To test this, we attempted to delete the *ftsH1* gene in the 2 T1 background (Fig. S5A). In wild-type cells, *ftsH1* is essential and cannot be deleted [23]. By contrast, *ftsH1* could now be deleted in the 2T1L1A1P1 mutant expressing recombinant FtsH1–3 × FLAG and, importantly, in the 2 T1 strain, in which the transmembrane domain of FtsH2 was replaced by that of FtsH1 (Fig. S5B and S5C). Lack of FtsH1 in these strains was further confirmed by PCR and immunoblotting (Fig. 6A and Fig. S5D). By contrast, deletion of *ftsH1* was not possible in the 2L1A1P1 background, further highlighting the non-redundant role of the FtsH1 transmembrane domain in supporting essential FtsH1/3 function in vivo (Fig. S5B).

We further tested FtsH1 functionality in these mutants using an established Fur in vivo degradation assay. Fur, a transcriptional repressor essential for iron homeostasis, is a direct substrate of the native FtsH1/3 protease complex. Under iron-limiting conditions, degradation of Fur by FtsH1/3 rapidly induces *isiA* expression, facilitating photosynthetic acclimation to iron deficiency [42]. To test whether the chimeric complexes retained this critical function, mutants 2 T1-Δ*ftsH1* and 2T1L1A1P1-Δ*ftsH1* were subjected to iron starvation, and Fur degradation and IsiA accumulation were monitored. As a negative control, we employed the previously described FtsH1down strain [17]. Unlike FtsH1down, mutants 2 T1-Δ*ftsH1* and 2T1L1A1P1-Δ*ftsH1* exhibited clear reductions in Fur protein levels under iron stress, accompanied by pronounced IsiA expression (Fig. 6B). These findings indicate that chimera 2 T1 can functionally substitute for native FtsH1 in this stress response. Furthermore, IsiA accumulation under iron starvation, a photoprotective response that dissipates excess energy and mitigates oxidative damage, was confirmed by a blue shift in cellular chlorophyll absorption [18]. Specifically, WT and both Δ*ftsH1* mutants exhibited a complete shift from 678 nm to 671 nm, indicative of rapid acclimation, whereas FtsH1down cells displayed a delayed and smaller shift to approximately 674 nm (Fig. 6C). Collectively, these data suggested that the transmembrane domain of FtsH1 is sufficient to support Fur degradation in this stress response.

3.6. The transmembrane domains of FtsH1 and FtsH2 are primary determinants of membrane localization

To test whether the transmembrane domains were responsible for targeting the FtsH complexes to the correct membrane, we generated a set of mutants expressing native and chimeric FtsH proteins with reciprocally exchanged transmembrane domains of FtsH1 and FtsH2 (Table S1). Except for WT and Δ*ftsH2*-GFP, all constructs contained superfolder Green Fluorescent Protein (GFP) fused to the C-terminus of FtsH via a flexible Gly4Ser (GGGGS) linker, allowing their subcellular localization to be monitored by confocal microscopy (Fig. 7). WT cells showed only chlorophyll fluorescence, whereas Δ*ftsH2*-GFP exhibited diffuse cytoplasmic GFP fluorescence. Control strains expressing FtsH1-GFP and FtsH2-GFP displayed distinct localization patterns corresponding to cytoplasmic and thylakoid membranes, respectively, consistent with previous findings [27]. Chimera 2 T1-GFP, in which the transmembrane domain of FtsH2 was replaced by that of FtsH1, exhibited fluorescence similar to FtsH1-GFP at the cytoplasmic membranes. By contrast, chimera 2L1A1P1-GFP, containing the soluble regions of FtsH1 but retaining the transmembrane domain of FtsH2, showed fluorescence matching the thylakoid membrane localization of FtsH2-GFP (Fig. 7). Collectively, these results demonstrate that the identity of the transmembrane domain plays a major role in the membrane localization of FtsH proteins.

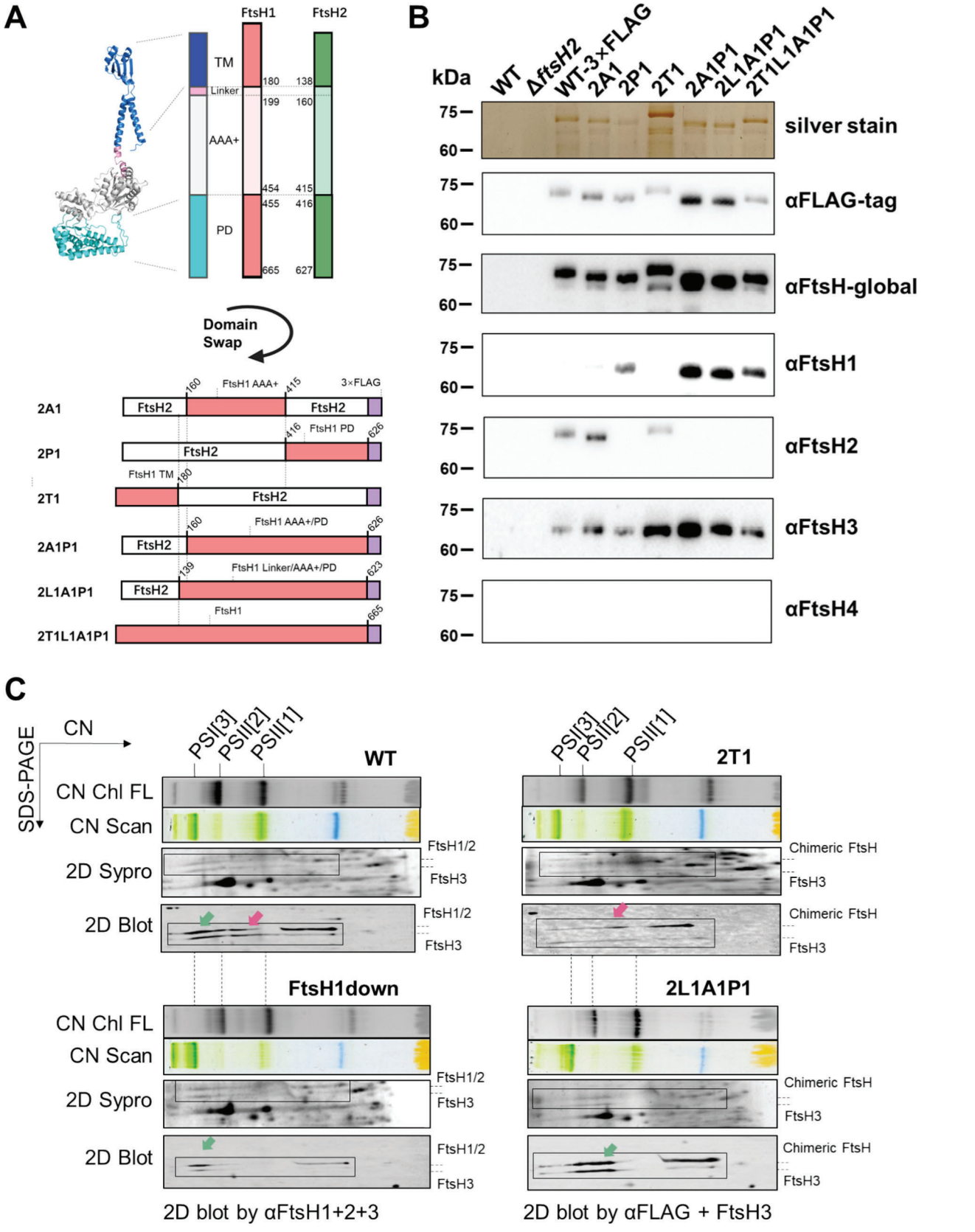

(caption on next page)

Fig. 4. Systematic domain swapping between FtsH1 and FtsH2 and analysis of chimeric FtsH complexes.
(A) The schematic at the top shows a single FtsH protomer (cartoon) and a linear map that defines the transmembrane domain (TM, navy), linker (pink), AAA+ domain (gray), and protease domain (PD, cyan). The adjoining bars align the domains of FtsH1 (magenta) and FtsH2 (green) with their residue boundaries labeled. Segments of FtsH1 were inserted into the FtsH2 backbone to create six chromosome-encoded chimeras: 2A1 (FtsH1 AAA+), 2P1 (FtsH1 PD), 2 T1 (FtsH1 TM), 2A1P1 (AAA+ and PD), 2L1A1P1 (FtsH1 linker, AAA+, and PD), and 2T1L1A1P1 (FtsH1 TM, linker, AAA+, and PD, representing the full-length FtsH1 sequence). Linear diagrams below highlight the donor segments (magenta) within each construct; all retain the remaining FtsH2 regions (white) and carry a C-terminal 3 × FLAG tag (purple) for purification. (B) Composition analysis of purified FtsH complexes by silver staining and immunoblotting with antibodies against the FLAG tag, all FtsH isoforms (αFtsH-global), and FtsH1–4. (C) Two-dimensional (2D) CN/SDS-PAGE analysis of membrane proteins isolated from WT, FtsH1down, and chimeric mutants. Membrane protein complexes were separated by CN-PAGE, scanned (CN Scan), and chlorophyll autofluorescence was recorded (CN Chl FL). Gel strips were subsequently separated by SDS-PAGE, and proteins were stained with SYPRO Orange as loading controls (2D Sypro). Positions of FtsH complexes are indicated by black rectangles. Red and green arrows indicate the positions of FtsH1/3 and FtsH2/3 complexes, respectively. Other labeled complexes: PSII [1], PSII [2], and PSI [3] denote PSII monomers, PSII dimers, and PSI trimers, respectively. (For interpretation of the references to colour in this figure legend, the reader is referred to the web version of this article.)

4. Discussion

Our work has revealed that the transmembrane domains of FtsH1 and FtsH2 play a major role in defining the location and substrate specificity of the FtsH1/3 and FtsH2/3 heterocomplexes in *Syn*6803. By contrast, the linker region and the AAA+ and protease modules did not have a dramatic impact on the function of the FtsH chimeric heterocomplexes. However, given that the complete spectrum of substrates for FtsH2/3 and FtsH1/3 is unknown, it remains possible that sequence differences in these regions might fine tune activity under certain conditions. Also, it is likely that relatively minor variations in sequence within closely related homologs, such as FtsH1 and FtsH2, may be tolerated but not in the case of modules in more distant phylogenetic groups. For instance, the native PaFtsH1 in *Pseudomonas aeruginosa*, which contains an additional GGG motif in the linker region, shows altered substrate specificity compared to the horizontally acquired xenolog PaFtsH2, in which artificial insertion of this motif broadens substrate specificity [10].

Previous studies have proposed that the membrane-proximal linker can modulate the position and mobility of the cytosolic region relative to the membrane, thereby altering the opening through which substrates reach the central pore [10,11]. Our simulations predicted distinct substrate-entry geometries for FtsH1/3 and FtsH2/3 complexes. Because the simulations examined the complete heterocomplexes, these differences cannot be attributed to linker sequence variation alone. Moreover, deletion of the GGP motif or replacement of the FtsH2 linker with that of FtsH1 produced no detectable changes in the light-growth or maltose-stress phenotypes. These findings suggest that the functional effects of linker variation may depend on the broader FtsH sequence context and substrate identity. For the closely related FtsH1 and FtsH2 paralogs in *Syn*6803, however, linker variation was not sufficient to account for functional divergence, whereas the transmembrane domain was the major determinant.

In the cases of FtsH1 and FtsH2, the transmembrane domain consists of two predicted transmembrane α-helices connected by a lumenal (in the case of FtsH2/3) or periplasmically exposed domain (FtsH1/3). For FtsH2, the 81-amino acid lumenal domain is uniquely present in FtsH proteins from oxygenic phototrophs, including *Arabidopsis* FtsH2 (VAR2) [43]. This domain, situated between two predicted transmembrane helices, may represent a structural adaptation linked to the specialized functions of FtsH proteases in photosynthetic membranes, including the processing of membrane substrates such as D1 [43].

How FtsH proteins are targeted to the thylakoid and cytoplasmic membranes in cyanobacteria is currently unclear. Detailed proteomic analyses suggest that subunits of the Sec/YidC and twin-arginine (Tat) translocation pathways involved in membrane protein insertion are located in the thylakoid membrane [44], although the SecY subunit has also been detected in the cytoplasmic membrane fraction of *Synechococcus* sp. PCC 7942 [45]. However, it remains possible that proteins destined for the cytoplasmic membrane are first inserted into specialized biogenic regions and then sorted [46].

In the case of Arabidopsis chloroplasts, in vitro import experiments suggest that the orthologs of FtsH2 (AtFtsH2 and AtFtsH8) rely on the Tat pathway for thylakoid membrane integration, while the orthologs of FtsH3 (AtFtsH1 and AtFtsH5) are inserted into the thylakoid via the Sec pathway [47]. Given that the cyanobacterial FtsH1 and FtsH2 subunits lack the canonical twin-arginine motif required for Tat-mediated insertion, the use of the Tat pathway to insert FtsH2 in the membrane is likely a new feature of plants. Moreover, the current data suggest that AtFtsH1, 2, 5 and 8 are N-terminally processed so that the transmembrane domain of the mature protein consists of only a single transmembrane helix with the exposed N-terminal region located in the thylakoid lumen [47]. In contrast, N-terminal sequencing indicates that the *Syn*6803 FtsH2/3/4 homologs are not processed and so contain two transmembrane helices [8], despite the presence of a putative A-X-A (X = any amino acid) cleavage site within the transmembrane domains (Fig. S6). Whether FtsH1 is N-terminally processed is currently unclear.

The mechanism by which FtsH proteases recognize and degrade cytoplasmic substrates like Fur and GgpS is also an open question. The FtsH1/3 complex primarily regulates Fur levels in its DNA-unbound, cytoplasmic form [18]. Similarly, GgpS, a known substrate of the FtsH2/3 complex, is a soluble cytoplasmic enzyme [48,49]. Given that the catalytic domains of both FtsH1/3 and FtsH2/3 complexes are exposed to the cytoplasm, both Fur and GgpS should, in principle, be accessible to either protease complex. Unexpectedly, the mutant expressing a chimeric FtsH2/3 complex anchored in the cytoplasmic membrane via the transmembrane domain of FtsH1 (chimera 2 T1) exhibited enhanced maltose tolerance despite retaining functional catalytic domains. This phenotype is consistent with altered FtsH2-dependent regulation of GgpS [20], although changes in GgpS turnover, expression, or activity, as well as other compensatory responses, could contribute to the observed tolerance. Conversely, the same chimera acquired the ability to degrade Fur. Together, these findings indicate that the transmembrane domain of FtsH2 is required to maintain WT-like sensitivity to maltose stress, whereas the transmembrane domain of FtsH1 is required for Fur degradation under iron stress. These observations suggest that differences in the linker, AAA+, and protease domains alone are insufficient to account for the distinct substrate specificities, whereas the identity of the transmembrane domain makes a major contribution. The transmembrane domains might confer specificity either by direct substrate recognition or indirectly through adaptor proteins such as prohibitins [50–52]. Alternatively, the spatial proximity between substrates and FtsH protease complexes could affect selective degradation [53,54]. Thus, differential subcellular localization of Fur and GgpS might influence their accessibility to FtsH1/3 and FtsH2/3 complexes, respectively.

Our study links sequence differences in the transmembrane domain to the targeting of FtsH heterocomplexes to either the cytoplasmic or thylakoid membranes. From an evolutionary perspective, the last common ancestor of present-day cyanobacteria had three FtsH paralogs that were ancestral to FtsH1/FtsH2, FtsH3 and FtsH4 [25]. *Gloeobacter* species, representing the earliest known lineage of cyanobacteria [55–57], do not possess a thylakoid membrane system but instead contain the photosynthetic apparatus in the cytoplasmic membrane [58], and

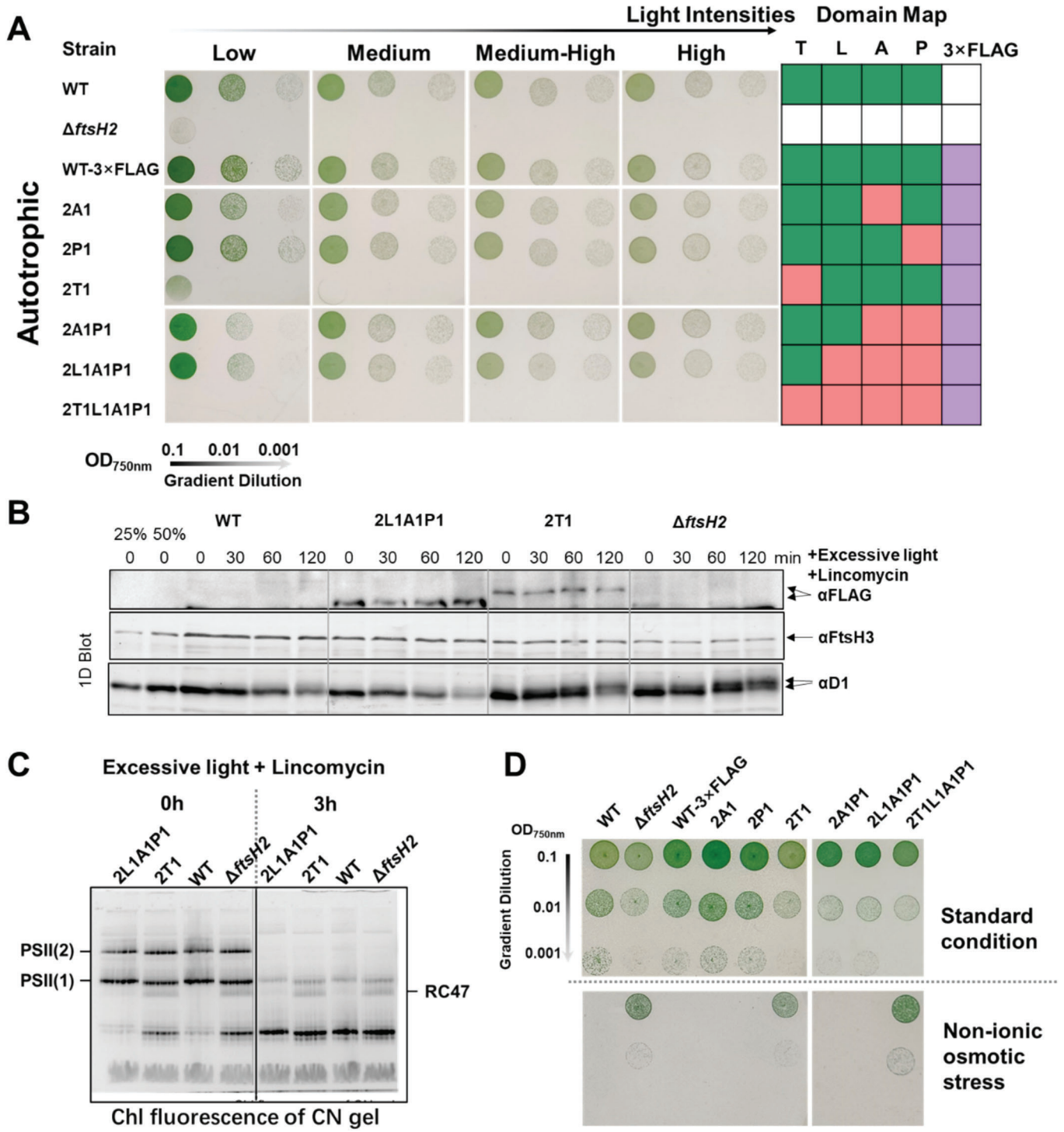

Fig. 5. Transmembrane domain swapping between FtsH1 and FtsH2 impairs FtsH2-mediated D1 turnover and enhances resistance to non-salt osmotic stress. (A) Spot growth assay under autotrophic conditions with the same four light intensities described in Fig. 1C. (B) SDS-PAGE and (C) CN-PAGE analyses of membranes isolated from WT, Δ*ftsH2*, and chimeric strains exposed to excessive light stress (500 μE m^{-2} s^{-1}) in the presence of lincomycin, a protein synthesis inhibitor. Samples were collected at indicated time points: 0, 30, 60, and 120 min (B), and 0 and 3 h (C). (B) Immunoblotting was performed using antibodies specific for FLAG, FtsH3, and the D1 protein. (C) CN-PAGE gels show chlorophyll fluorescence indicative of different PSII complexes before and after excessive high-light exposure. PSII (2), dimeric PSII; PSII (1), monomeric PSII; RC47, PSII monomer lacking CP43. (D) Spot growth assay under maltose-induced osmotic stress conditions.

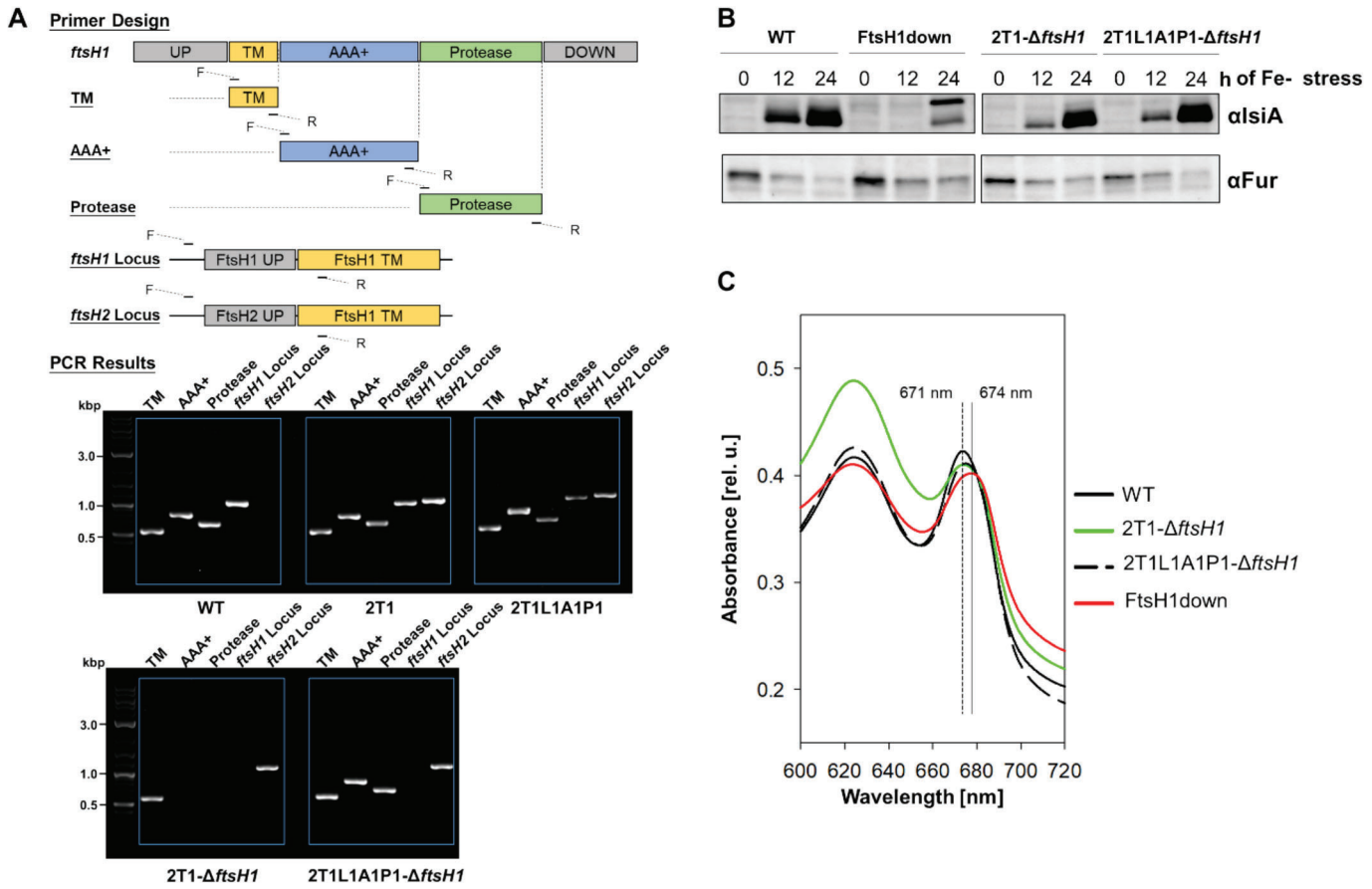

Fig. 6. Chimeric FtsH protein bearing the FtsH1 transmembrane domain rescues FtsH1-dependent stress responses.
(A) PCR verification of stable deletion of native *ftsH1*. Mutant strains were maintained for >4 months on antibiotic-free plates after purification. Five primer sets (schematically shown) were designed to detect residual *ftsH1* fragments: three targeting the transmembrane (TM), AAA+, and protease domains, respectively, and two specifically distinguishing native *ftsH1* locus fragments from integrated chimeric sequences at the *ftsH2* locus (mutants 2 T1 and 2T1L1A1P1 contain *ftsH1*-derived sequences). (B) Immunoblot analyses of crude membrane fractions isolated from cells harvested at 0, 12, and 24 h under iron starvation. Anti-IsiA and anti-Fur antibodies were used to monitor IsiA accumulation and Fur degradation under iron-limiting conditions. (C) Absorption spectra of WT, FtsH1down, 2 T1-Δ*ftsH1*, and 2T1L1A1P1-Δ*ftsH1* strains after 24 h of iron starvation. Cells were adjusted to an OD750 of 0.2, and absorption spectra (600–720 nm) were measured and normalized to the chlorophyll red absorption peak at 680 nm. (For interpretation of the references to colour in this figure legend, the reader is referred to the web version of this article.)

notably lack clear FtsH1 and FtsH2 orthologs (Table S2) [25]. The *Thermostichaceae* lineage, the earliest known cyanobacterial group with a thylakoid membrane system [59], is the only lineage with thylakoids that lacks distinct FtsH1 and FtsH2 paralogs (Table S2). This suggests that the divergence of FtsH1 and FtsH2 likely occurred after the emergence of thylakoid membranes and may have facilitated specialized protein degradation in the two distinct membrane systems. Interestingly, the conserved residues within the lumenal/periplasmic domain of the undifferentiated FtsH1/2 homologs in *Gloeobacter* and *Thermostichaceae* align more closely with those specific to cyanobacterial FtsH2 (Fig. S7).

5. Conclusions

This study shows that the transmembrane domains of FtsH1 and FtsH2 are major determinants of the membrane localization and substrate specificity of the FtsH1/3 and FtsH2/3 heterocomplexes in *Synechocystis* sp. PCC 6803. By contrast, the soluble regions, including the linker, AAA+ ATPase domain and protease domain, were largely interchangeable under the conditions tested. Replacing the FtsH2 transmembrane domain with that of FtsH1 shifted the localization of the resulting chimera toward the cytoplasmic membrane. This substitution compromised FtsH2/3-associated functions, including D1 turnover during PSII repair and the non-salt osmotic-stress phenotype associated with GgpS regulation, while allowing the chimera to support FtsH1-dependent Fur degradation and iron-stress acclimation. Together, these findings show that variation in the transmembrane domain can link membrane targeting to substrate-specific function without requiring corresponding divergence in the conserved catalytic machinery responsible for substrate entry, unfolding, and degradation.

Our results further support a model in which localization specified by the transmembrane domain may shape substrate access and thereby contribute to the functional specialization of cyanobacterial FtsH heterocomplexes. Whether the transmembrane domains contribute directly to substrate recognition or act indirectly by altering substrate proximity or interactions with associated protein factors remains to be determined. In an evolutionary context, divergence of the transmembrane domains after duplication of the FtsH1/FtsH2 ancestor may have promoted the specialization of FtsH-mediated proteolysis between the cytoplasmic and thylakoid membranes.

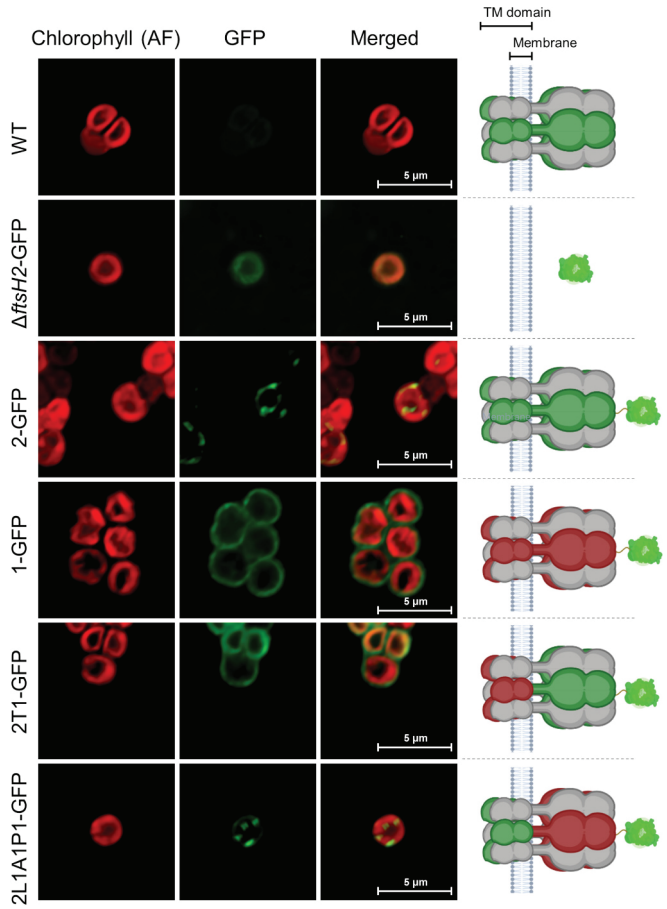

Fig. 7. Transmembrane domain swapping between FtsH1 and FtsH2 alters FtsH localization.
Confocal microscopy images show chlorophyll autofluorescence (Chl, red), GFP fluorescence (green), and merged signals in WT and five GFP-tagged mutants. The domain map summarizes genetic modifications used to generate each FtsH-GFP chimera corresponding to strains shown on the left. Detailed strain genotypes are provided in Table S1. The schematic on the right illustrates the corresponding colour model representing FtsH hexamers composed of FtsH1 (burgundy), FtsH2 (green), and their chimeras in combination with the FtsH3 protomer (light gray). GFP is shown in fluorescent green. All FtsH complexes are anchored to the membrane (blue). (For interpretation of the references to colour in this figure legend, the reader is referred to the web version of this article.)

CRediT authorship contribution statement

Lanbo Yi: Writing – review & editing, Writing – original draft, Visualization, Validation, Methodology, Investigation, Formal analysis, Conceptualization. **Natalia Kulik:** Writing – review & editing, Visualization, Resources, Methodology, Investigation, Formal analysis. **Shengxi Shao:** Resources, Formal analysis. **Peter J. Nixon:** Writing – review & editing, Supervision, Project administration, Funding acquisition, Formal analysis, Conceptualization. **Josef Komenda:** Writing – review & editing, Supervision, Project administration, Funding acquisition, Formal analysis, Conceptualization. **Vendula Krynická:** Writing – review & editing, Writing – original draft, Visualization, Validation, Supervision, Resources, Project administration, Methodology, Investigation, Funding acquisition, Formal analysis, Conceptualization. **Jianfeng Yu:** Writing – review & editing, Writing – original draft, Supervision, Resources, Project administration, Methodology, Investigation, Formal analysis, Conceptualization. **Bin Liu:** Supervision, Resources, Project administration, Funding acquisition, Formal analysis, Conceptualization.

Funding

This work was supported by the Youth Taishan Scholarship Project [grant number tsqnz20240812]; the Shenzhen Science and Technology Program [grant number KQTD20180412181334790]; the Guangdong Province Zhujiang Talent Program [grant number 2019ZT08H476]; the Biotechnology and Biological Sciences Research Council [grant number BB/V002007/1]; the European Research Council (ERC)-Synergy Grant [grant number 854126]; the Ministry of Education, Youth and Sports of the Czech Republic [grant number CZ.02.01.01/00/22_008/0004624]; the Czech Science Foundation [grant number 25-17569S]; and the National Natural Science Foundation of China [grant number 32360911].

Declaration of competing interest

The authors declare that they have no known competing financial interests or personal relationships that could have appeared to influence the work reported in this paper.

Acknowledgments

We dedicate this paper to the memory of Prof. Feng Chen, who passed away during the course of this project. We gratefully acknowledge the valuable support and guidance he provided for this work.

Appendix A. Supplementary data

Supplementary data to this article can be found online at https://doi.org/10.1016/j.algal.2026.104894.

Data availability

The data supporting the findings of this study are included in the article and its supplementary material.

References

[1] L. Yi, B. Liu, P.J. Nixon, J. Yu, F. Chen, Recent advances in understanding the structural and functional evolution of FtsH proteases, Front. Plant Sci. 13 (2022) 837528, https://doi.org/10.3389/fpls.2022.837528.
[2] K. Ito, Y. Akiyama, Cellular functions, mechanism of action, and regulation of FtsH protease, Ann. Rev. Microbiol. 59 (2005) 211–231, https://doi.org/10.1146/annurev.micro.59.030804.121316.
[3] R. Suno, H. Niwa, D. Tsuchiya, X. Zhang, M. Yoshida, K. Morikawa, Structure of the whole cytosolic region of ATP-dependent protease FtsH, Mol. Cell 22 (2006) 575–585, https://doi.org/10.1016/j.molcel.2006.04.020.
[4] C. Puchades, A.J. Rampello, M. Shin, C.J. Giuliano, R.L. Wiseman, S.E. Glynn, G. C. Lander, Structure of the mitochondrial inner membrane AAA+ protease YME1 gives insight into substrate processing, Science 358 (2017) eaao0464, https://doi.org/10.1126/science.aao0464.
[5] S. Lee, S. Augustin, T. Tatsuta, F. Gerdes, T. Langer, F.T.F. Tsai, Electron cryomicroscopy structure of a membrane-anchored mitochondrial AAA protease, J. Biol. Chem. 286 (2011) 4404–4411, https://doi.org/10.1074/jbc.M110.158741.
[6] M. Ferro, S. Brugière, D. Salvi, D. Seigneurin-Berny, M. Court, L. Moyet, C. Ramus, S. Miras, M. Mellal, S. Le Gall, S. Kieffer-Jaquinod, C. Bruley, J. Garin, J. Joyard, C. Masselon, N. Rolland, AT_CHLORO, a comprehensive chloroplast proteome database with subplastidial localization and curated information on envelope proteins, Mol. Cell. Proteomics 9 (2010) 1063–1084, https://doi.org/10.1074/mcp.M900325-MCP200.
[7] R. Wagner, H. Aigner, C. Funk, FtsH proteases located in the plant chloroplast, Physiol. Plant. 145 (2012) 203–214, https://doi.org/10.1111/j.1399-3054.2011.01548.x.
[8] M. Boehm, J. Yu, V. Krynicka, M. Barker, M. Tichy, J. Komenda, P.J. Nixon, J. Nield, Subunit organization of a *Synechocystis* hetero-oligomeric thylakoid FtsH complex involved in photosystem II repair, Plant Cell 24 (2012) 3669–3683, https://doi.org/10.1105/tpc.112.100891.
[9] K. Leonhard, J.M. Herrmann, R.A. Stuart, G. Mannhaupt, W. Neupert, T. Langer, AAA proteases with catalytic sites on opposite membrane surfaces comprise a proteolytic system for the ATP-dependent degradation of inner membrane proteins in mitochondria, EMBO J. 15 (1996) 4218–4229, https://doi.org/10.1002/j.1460-2075.1996.tb00796.x.
[10] G.D. Mawla, S.M. Kamal, L.-Y. Cao, P. Purhonen, H. Hebert, R.T. Sauer, T.A. Baker, U. Römling, The membrane-cytoplasmic linker defines activity of FtsH proteases in *Pseudomonas aeruginosa* clone C, J. Biol. Chem. 300 (2024) 105622, https://doi.org/10.1016/j.jbc.2023.105622.

[11] V. Carvalho, I. Prabudiansyah, L. Kovacik, M. Chami, R. Kieffer, R. van der Valk, N. de Lange, A. Engel, M.-E. Aubin-Tam, The cytoplasmic domain of the AAA+ protease FtsH is tilted with respect to the membrane to facilitate substrate entry, J. Biol. Chem. 296 (2021) 100029, https://doi.org/10.1074/jbc.RA120.014739.
[12] Y. Akiyama, K. Ito, Roles of multimerization and membrane association in the proteolytic functions of FtsH (HflB), EMBO J. 19 (2000) 3888–3895, https://doi.org/10.1093/emboj/19.15.3888.
[13] D. Korbel, S. Wurth, M. Käser, T. Langer, Membrane protein turnover by the *m*-AAA protease in mitochondria depends on the transmembrane domains of its subunits, EMBO Rep. 5 (2004) 698–703, https://doi.org/10.1038/sj.embor.7400186.
[14] Y. Akiyama, T. Yoshihisa, K. Ito, FtsH, a membrane-bound ATPase, forms a complex in the cytoplasmic membrane of *Escherichia coli*, J. Biol. Chem. 270 (1995) 23485–23490, https://doi.org/10.1074/jbc.270.40.23485.
[15] M. Graef, G. Seewald, T. Langer, Substrate recognition by AAA+ ATPases: distinct substrate binding modes in ATP-dependent protease Yme1 of the mitochondrial intermembrane space, Mol. Cell. Biol. 27 (2007) 2476–2485, https://doi.org/10.1128/MCB.01721-06.
[16] V. Krynická, J. Komenda, The role of FtsH complexes in the response to abiotic stress in cyanobacteria, Plant Cell Physiol. 65 (2024) 1103–1114, https://doi.org/10.1093/pcp/pcae042.
[17] V. Krynická, J. Georg, P.J. Jackson, M.J. Dickman, C.N. Hunter, M.E. Futschik, W. R. Hess, J. Komenda, Depletion of the FtsH1/3 proteolytic complex suppresses the nutrient stress response in the cyanobacterium *Synechocystis* sp strain PCC 6803, Plant Cell 31 (2019) 2912–2928, https://doi.org/10.1105/tpc.19.00411.
[18] V. Krynická, M. Tichý, J. Krafl, J. Yu, R. Kaňa, M. Boehm, P.J. Nixon, J. Komenda, Two essential FtsH proteases control the level of the Fur repressor during iron deficiency in the cyanobacterium *Synechocystis* sp. PCC 6803, Mol. Microbiol. 94 (2014) 609–624, https://doi.org/10.1111/mmi.12782.
[19] P.J. Nixon, M. Barker, M. Boehm, R. de Vries, J. Komenda, FtsH-mediated repair of the photosystem II complex in response to light stress, J. Exp. Bot. 56 (2005) 357–363, https://doi.org/10.1093/jxb/eri021.
[20] M. Stirnberg, S. Fulda, J. Huckauf, M. Hagemann, R. Krämer, K. Marin, A membrane-bound FtsH protease is involved in osmoregulation in *Synechocystis* sp. PCC 6803: the compatible solute synthesizing enzyme GgpS is one of the targets for proteolysis, Mol. Microbiol. 63 (2007) 86–102, https://doi.org/10.1111/j.1365-2958.2006.05495.x.
[21] V. Krynická, P. Skotnicová, P.J. Jackson, S. Barnett, J. Yu, A. Wysocka, R. Kaňa, M. J. Dickman, P.J. Nixon, C.N. Hunter, J. Komenda, FtsH4 protease controls biogenesis of the PSII complex by dual regulation of high light-inducible proteins, Plant Commun. 4 (2023) 100502, https://doi.org/10.1016/j.xplc.2022.100502.
[22] P. Koník, P. Skotnicová, S. Gupta, M. Tichý, S. Sharma, J. Komenda, R. Sobotka, V. Krynická, The cyanobacterial FtsH4 protease controls accumulation of protein factors involved in the biogenesis of photosystem I, Biochim. Biophys. Acta Bioenerg. 1865 (2024) 149017, https://doi.org/10.1016/j.bbabio.2023.149017.
[23] N.H. Mann, N. Novac, C.W. Mullineaux, J. Newman, S. Bailey, C. Robinson, Involvement of an FtsH homologue in the assembly of functional photosystem I in the cyanobacterium *Synechocystis* sp. PCC 6803, FEBS Lett. 479 (2000) 72–77, https://doi.org/10.1016/S0014-5793(00)01871-8.
[24] P. Silva, E. Thompson, S. Bailey, O. Kruse, C.W. Mullineaux, C. Robinson, N. H. Mann, P.J. Nixon, FtsH is involved in the early stages of repair of photosystem II in *Synechocystis* sp PCC 6803, Plant Cell 15 (2003) 2152–2164, https://doi.org/10.1105/tpc.012609.
[25] S. Shao, T. Cardona, P.J. Nixon, Early emergence of the FtsH proteases involved in photosystem II repair, Photosynthetica 56 (2018) 163–177, https://doi.org/10.1007/s11099-018-0769-9.
[26] J. Yu, J. Knoppová, F. Michoux, W. Bialek, E. Cota, M.K. Shukla, A. Strašková, G. Pascual Aznar, R. Sobotka, J. Komenda, J.W. Murray, P.J. Nixon, Ycf48 involved in the biogenesis of the oxygen-evolving photosystem II complex is a seven-bladed beta-propeller protein, Proc. Natl. Acad. Sci. USA 115 (2018) E7824–E7833, https://doi.org/10.1073/pnas.1800609115.
[27] J. Sacharz, S.J. Bryan, J. Yu, N.J. Burroughs, E.M. Spence, P.J. Nixon, C. W. Mullineaux, Sub-cellular location of FtsH proteases in the cyanobacterium *Synechocystis* sp. PCC 6803 suggests localised PSII repair zones in the thylakoid membranes, Mol. Microbiol. 96 (2015) 448–462, https://doi.org/10.1111/mmi.12940.
[28] R.J. Porra, W.A. Thompson, P.E. Kriedemann, Determination of accurate extinction coefficients and simultaneous equations for assaying chlorophylls a and b extracted with four different solvents: verification of the concentration of chlorophyll standards by atomic absorption spectroscopy, Biochim. Biophys. Acta Bioenerg. 975 (1989) 384–394, https://doi.org/10.1016/S0005-2728(89)80347-0.
[29] J. Komenda, V. Krynická, T. Zakar, Isolation of thylakoid membranes from the cyanobacterium *Synechocystis* sp. PCC 6803 and analysis of their photosynthetic pigment-protein complexes by clear native-PAGE, Bio-Protoc. 9 (2019) e3126, https://doi.org/10.21769/BioProtoc.3126.
[30] J. Komenda, M. Tichý, L.A. Eichacker, The PsbH protein is associated with the inner antenna CP47 and facilitates D1 processing and incorporation into PSII in the cyanobacterium *Synechocystis* PCC 6803, Plant Cell Physiol. 46 (2005) 1477–1483, https://doi.org/10.1093/pcp/pci159.
[31] J. Abramson, J. Adler, J. Dunger, R. Evans, T. Green, A. Pritzel, O. Ronneberger, L. Willmore, A.J. Ballard, J. Bambrick, S.W. Bodenstein, D.A. Evans, C.-C. Hung, M. O'Neill, D. Reiman, K. Tunyasuvunakool, Z. Wu, A. Žemgulytė, E. Arvaniti, C. Beattie, O. Bertolli, A. Bridgland, A. Cherepanov, M. Congreve, A.I. Cowen-Rivers, A. Cowie, M. Figurnov, F.B. Fuchs, H. Gladman, R. Jain, Y.A. Khan, C.M. R. Low, K. Perlin, A. Potapenko, P. Savy, S. Singh, A. Stecula, A. Thillaisundaram, C. Tong, S. Yakneen, E.D. Zhong, M. Zielinski, A. Žídek, V. Bapst, P. Kohli, M. Jaderberg, D. Hassabis, J.M. Jumper, Accurate structure prediction of biomolecular interactions with AlphaFold 3, Nature 630 (2024) 493–500, https://doi.org/10.1038/s41586-024-07487-w.
[32] A. Šali, T.L. Blundell, Comparative protein modelling by satisfaction of spatial restraints, J. Mol. Biol. 234 (1993) 779–815, https://doi.org/10.1006/jmbi.1993.1626.
[33] H. Land, M.S. Humble, YASARA: A tool to obtain structural guidance in biocatalytic investigations, in: U.T. Bornscheuer, M. Höhne (Eds.), Protein Eng. Methods Protoc, Springer New York, New York, NY, 2018, pp. 43–67, https://doi.org/10.1007/978-1-4939-7366-8_4.
[34] M.A. Lomize, I.D. Pogozheva, H. Joo, H.I. Mosberg, A.L. Lomize, OPM database and PPM web server: resources for positioning of proteins in membranes, Nucleic Acids Res. 40 (2012) D370–D376, https://doi.org/10.1093/nar/gkr703.
[35] J. Lee, D.S. Patel, J. Ståhle, S.-J. Park, N.R. Kern, S. Kim, J. Lee, X. Cheng, M. A. Valvano, O. Holst, Y.A. Knirel, Y. Qi, S. Jo, J.B. Klauda, G. Widmalm, W. Im, CHARMM-GUI membrane builder for complex biological membrane simulations with glycolipids and lipoglycans, J. Chem. Theory Comput. 15 (2019) 775–786, https://doi.org/10.1021/acs.jctc.8b01066.
[36] J. Lee, M. Hitzenberger, M. Rieger, N.R. Kern, M. Zacharias, W. Im, CHARMM-GUI supports the Amber force fields, J. Chem. Phys. 153 (2020) 035103, https://doi.org/10.1063/5.0012280.
[37] S. Park, Y.K. Choi, S. Kim, J. Lee, W. Im, CHARMM-GUI membrane builder for lipid nanoparticles with ionizable cationic lipids and PEGylated lipids, J. Chem. Inf. Model. 61 (2021) 5192–5202, https://doi.org/10.1021/acs.jcim.1c00770.
[38] M.J. Abraham, T. Murtola, R. Schulz, S. Páll, J.C. Smith, B. Hess, E. Lindahl, GROMACS: high performance molecular simulations through multi-level parallelism from laptops to supercomputers, SoftwareX 1–2 (2015) 19–25, https://doi.org/10.1016/j.softx.2015.06.001.
[39] S. Páll, M.J. Abraham, C. Kutzner, B. Hess, E. Lindahl, Tackling exascale software challenges in molecular dynamics simulations with GROMACS, in: S. Markidis, E. Laure (Eds.), Solving Softw. Chall, Exascale, Springer International Publishing, Cham, 2015, pp. 3–27.
[40] L. Lupínková, J. Komenda, Oxidative modifications of the photosystem II D1 protein by reactive oxygen species: from isolated protein to cyanobacterial cells, Photochem. Photobiol. 79 (2004) 152–162, https://doi.org/10.1111/j.1751-1097.2004.tb00005.x.
[41] J. Komenda, M. Barker, S. Kuviková, R. de Vries, C.W. Mullineaux, M. Tichý, P. J. Nixon, The FtsH protease slr0228 is important for quality control of photosystem II in the thylakoid membrane of *Synechocystis* sp, PCC 6803,, J. Biol. Chem. 281 (2006) 1145–1151, https://doi.org/10.1074/jbc.M503852200.
[42] Q. Wang, C.L. Hall, M.Z. Al-Adami, Q. He, IsiA is required for the formation of photosystem I supercomplexes and for efficient state transition in *Synechocystis* PCC 6803, PLoS One 5 (2010) e10432, https://doi.org/10.1371/journal.pone.0010432.
[43] S. Bailey, E. Thompson, P.J. Nixon, P. Horton, C.W. Mullineaux, C. Robinson, N. H. Mann, A critical role for the Var2 FtsH homologue of *Arabidopsis thaliana* in the photosystem II repair cycle *in vivo*, J. Biol. Chem. 277 (2002) 2006–2011, https://doi.org/10.1074/jbc.M105878200.
[44] L.L. Baers, L.M. Breckels, L.A. Mills, L. Gatto, M.J. Deery, T.J. Stevens, C.J. Howe, K.S. Lilley, D.J. Lea-Smith, Proteome mapping of a cyanobacterium reveals distinct compartment organization and cell-dispersed metabolism, Plant Physiol. 181 (2019) 1721–1738, https://doi.org/10.1104/pp.19.00897.
[45] M. Nakai, D. Sugita, T. Omata, T. Endo, Sec-Y protein is localized in both the cytoplasmic and thylakoid membranes in the cyanobacterium *Synechococcus* PCC7942, Biochem. Biophys. Res. Commun. 193 (1993) 228–234, https://doi.org/10.1006/bbrc.1993.1613.
[46] A. Rast, M. Schaffer, S. Albert, W. Wan, S. Pfeffer, F. Beck, J.M. Plitzko, J. Nickelsen, B.D. Engel, Biogenic regions of cyanobacterial thylakoids form contact sites with the plasma membrane, Nat. Plants 5 (2019) 436–446, https://doi.org/10.1038/s41477-019-0399-7.
[47] R.A.O. Rodrigues, M.C. Silva-Filho, K. Cline, FtsH2 and FtsH5: two homologous subunits use different integration mechanisms leading to the same thylakoid multimeric complex, Plant J. 65 (2011) 600–609, https://doi.org/10.1111/j.1365-313X.2010.04448.x.
[48] M. Hagemann, U. Effmert, T. Kerstan, A. Schoor, N. Erdmann, Biochemical characterization of glucosylglycerol-phosphate synthase of *Synechocystis* sp. strain PCC 6803: comparison of crude, purified, and recombinant enzymes, Curr. Microbiol. 43 (2001) 278–283, https://doi.org/10.1007/s002840010301.
[49] J.F. Novak, M. Stirnberg, B. Roenneke, K. Marin, A novel mechanism of osmosensing, a salt-dependent protein-nucleic acid interaction in the cyanobacterium *Synechocystis* species PCC 6803, J. Biol. Chem. 286 (2011) 3235–3241, https://doi.org/10.1074/jbc.M110.157032.
[50] G. Steglich, W. Neupert, T. Langer, Prohibitins regulate membrane protein degradation by the *m*-AAA protease in mitochondria, Mol. Cell. Biol. 19 (1999) 3435–3442, https://doi.org/10.1128/MCB.19.5.3435.
[51] C. Ma, C. Wang, D. Luo, L. Yan, W. Yang, N. Li, N. Gao, Structural insights into the membrane microdomain organization by SPFH family proteins, Cell Res. 32 (2022) 176–189, https://doi.org/10.1038/s41422-021-00598-3.
[52] M. Boehm, J. Nield, P. Zhang, E.-M. Aro, J. Komenda, P.J. Nixon, Structural and mutational analysis of band 7 proteins in the cyanobacterium *Synechocystis* sp. strain PCC 6803, J. Bacteriol. 191 (2009) 6425–6435, https://doi.org/10.1128/jb.00644-09.
[53] A. Wilson, G. Ajlani, J.-M. Verbavatz, I. Vass, C.A. Kerfeld, D. Kirilovsky, A soluble carotenoid protein involved in phycobilisome-related energy dissipation in cyanobacteria, Plant Cell 18 (2006) 992–1007, https://doi.org/10.1105/tpc.105.040121.

[54] B. Lim, R. Miyazaki, S. Neher, D.A. Siegele, K. Ito, P. Walter, Y. Akiyama, T. Yura, C.A. Gross, Heat shock transcription factor σ^{32} co-opts the signal recognition particle to regulate protein homeostasis in *E. coli*, PLoS Biol. 11 (2013) e1001735, https://doi.org/10.1371/journal.pbio.1001735.

[55] C.E. Blank, P. Sánchez-Baracaldo, Timing of morphological and ecological innovations in the cyanobacteria – a key to understanding the rise in atmospheric oxygen, Geobiology 8 (2010) 1–23, https://doi.org/10.1111/j.1472-4669.2009.00220.x.

[56] J.H.W. Saw, M. Schatz, M.V. Brown, D.D. Kunkel, J.S. Foster, H. Shick, S. Christensen, S. Hou, X. Wan, S.P. Donachie, Cultivation and complete genome sequencing of *Gloeobacter kilaueensis* sp. nov., from a lava cave in Kīlauea Caldera, Hawai'i, PLoS One 8 (2013) e76376, https://doi.org/10.1371/journal.pone.0076376.

[57] A.Y. Mulkidjanian, E.V. Koonin, K.S. Makarova, S.L. Mekhedov, A. Sorokin, Y. I. Wolf, A. Dufresne, F. Partensky, H. Burd, D. Kaznadzey, R. Haselkorn, M. Y. Galperin, The cyanobacterial genome core and the origin of photosynthesis, Proc. Natl. Acad. Sci. USA 103 (2006) 13126–13131, https://doi.org/10.1073/pnas.0605709103.

[58] S. Rexroth, C.W. Mullineaux, D. Ellinger, E. Sendtko, M. Rögner, F. Koenig, The plasma membrane of the cyanobacterium *Gloeobacter violaceus* contains segregated bioenergetic domains, Plant Cell 23 (2011) 2379–2390, https://doi.org/10.1105/tpc.111.085779.

[59] S. Tan, L. Liu, J.-Y. Jiao, M.-M. Li, C.-J. Hu, A.-P. Lv, Y.-L. Qi, Y.-X. Li, Y.-Z. Rao, Y.-N. Qu, H.-C. Jiang, R.M. Soo, P.N. Evans, Z.-S. Hua, W.-J. Li, Exploring the origins and evolution of oxygenic and anoxygenic photosynthesis in deeply branched Cyanobacteriota, Mol. Biol. Evol. 41 (2024) msae151, https://doi.org/10.1093/molbev/msae151.